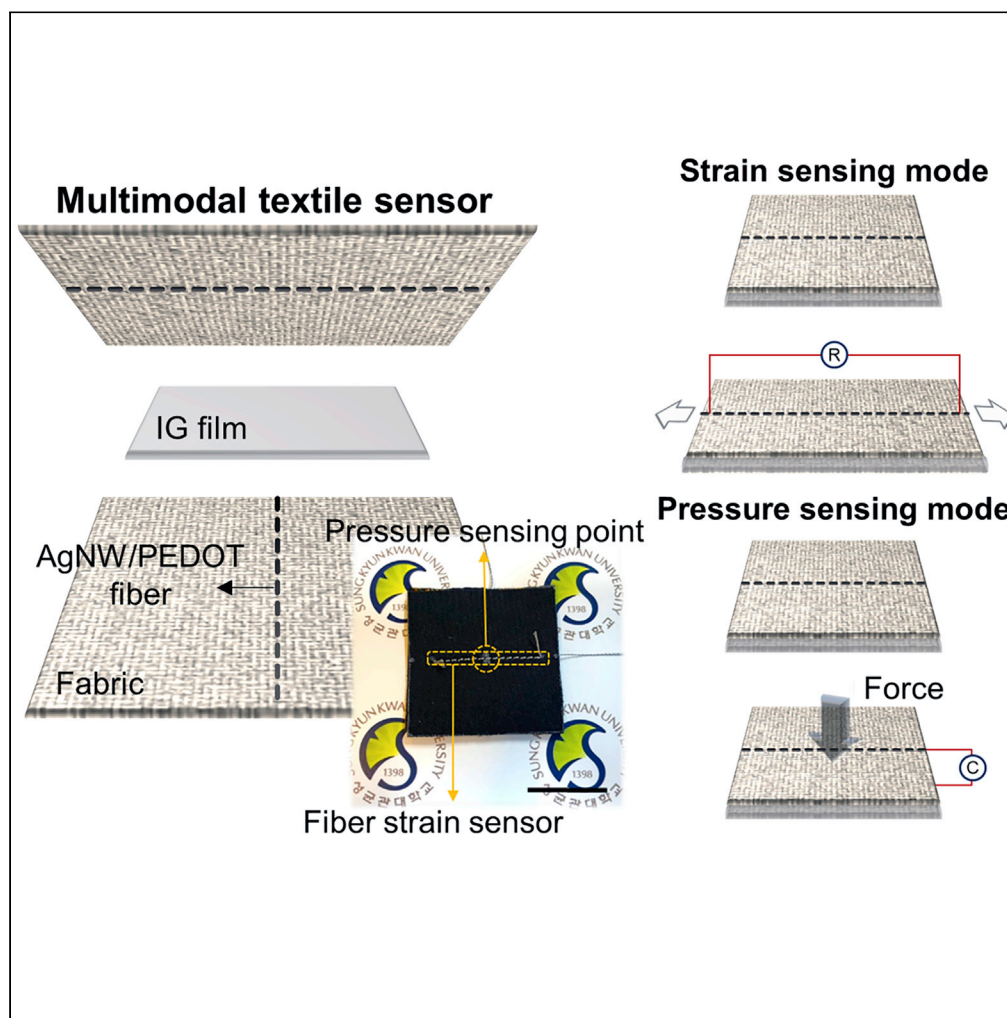**Article**

Mechanically robust textile-based strain and pressure multimodal sensors using metal nanowire/polymer conducting fibers

Kyobin Keum,
Sung Soo Cho,
Jeong-Wan Jo,
Sung Kyu Park,
Yong-Hoon Kim

yhkim76@skku.edu (Y.-H.K.)
skpark@cau.ac.kr (S.K.P.)

Highlights

Independent detection of strain and pressure using textile-based multimodal sensors

A high-*k* flexible ion-gel film is utilized for capacitive pressure sensing

Mechanically sewn conducting fibers are utilized for resistive strain sensing

Multimodal sensor detects multiple objects with different weights

iScience

Article

Mechanically robust textile-based strain and pressure multimodal sensors using metal nanowire/polymer conducting fibers

Kyobin Keum,[1] Sung Soo Cho,[2] Jeong-Wan Jo,[3] Sung Kyu Park,[2,*] and Yong-Hoon Kim[1,4,*]

SUMMARY

Recently, multifunctional textile-based sensory systems have attracted a lot of attention because of the growing demand for wearable electronics performing real-time monitoring of various body signals and movements. In particular, textile-based physical sensors often require multimodal sensing capabilities to accurately detect and identify multiple mixed stimuli simultaneously. Here, we demonstrate a textile-based strain/pressure multimodal sensor using high-*k* poly(vinylidene fluoride)-co-hexafluoropropylene ion-gel film and silver nanowire/poly(3,4-ethylenedioxythiophene):polystyrene sulfonate-coated conducting fibers. The multimodal sensors exhibited reliable strain and pressure-sensing characteristics for strain ranges up to 25% and pressures up to 50 kPa, respectively, with a relatively high strain gauge factor (up to 2.74) and pressure sensitivity (0.32 kPa^{-1}). More importantly, the textile-based multimodal sensor was able to detect the strain and pressure independently, allowing facile discrimination of strain and pressure. Using this approach, we demonstrated a textile-based multimodal sensor that incorporates one strain sensor and two pressure sensors detecting multiple weights simultaneously.

INTRODUCTION

Recently, wearable electronics have gained considerable interest owing to their wide applicability in emerging electronics such as real-time health/disease monitoring (Zhu et al., 2017; Kang et al., 2016), on-body electronic skin (You et al., 2021), and bioinspired robotic systems (Luo et al., 2021). Wearable electronics can be realized on various material platforms including ultrathin polymer substrates (Chen et al., 2019), stretchable elastomers (Trung et al., 2016), and textiles (Ho et al., 2019; Eom et al., 2017a), depending on their target applications. In particular, the textile-based wearable electronics hold a great promise owing to their unique physical characteristics such as compatibility with common clothing, light weight, softness, and inherent snug properties (Keum et al., 2021a). For these reasons, various sensor devices have been demonstrated on textile platform including pressure (Pyo et al., 2019; Lee et al., 2015), strain (Kim et al., 2021; Eom et al., 2017b), temperature (Wu et al., 2019), and humidity sensors (Zhou et al., 2017; Ma et al., 2019). More recently, in addition to these single-mode type sensor devices, multimodal textile sensors capable of detecting multiple stimuli were demonstrated (Wu et al., 2019; Chen et al., 2021). Because various stimuli are applied simultaneously (*cf.* a combination of strain with pressure) in usual operation conditions, multimodal sensing capability is highly demanded to achieve multifunctionality and to widen the utilization of textile sensors in various application areas. Previously, several multimodal sensory systems have been demonstrated on textile platforms. For instance, Agcayazi et al. reported a textile sensor array detecting pressure, humidity, and wetness (Agcayazi et al., 2020). By using a capacitive structure with insulating knit or meltblown textile as a dielectric, multiple stimuli could be identified by analyzing the capacitance or impedance variation. In addition, Yang et al. demonstrated multifunctional sensors using carbon-coated textiles which can detect strain, humidity, and temperature signals (Yang et al., 2021). Moreover, Qi et al. reported multimodal wearable textile sensors detecting pressure, stretching, and bending, utilizing carbon nanotube-embedded nanofiber yarns (Qi et al., 2020).

In multimodal sensors, one of the major concerns is the identification of individual stimulus from mixed stimuli. Particularly, because the stimuli such as strain and pressure can affect the output signals of each

[1]School of Advanced Materials Science and Engineering, Sungkyunkwan University, Suwon 16419, Republic of Korea

[2]School of Electrical and Electronics Engineering, Chung-Ang University, Seoul 06974, Republic of Korea

[3]Department of Electrical Engineering, University of Cambridge, CB2 1TN Cambridge, UK

[4]Lead contact

*Correspondence:
yhkim76@skku.edu (Y.-H.K.),
skpark@cau.ac.kr (S.K.P.)

https://doi.org/10.1016/j.isci.2022.104032

other, precise determination of each stimulation might be difficult unless a proper discrimination of the sensing signals is performed. In fact, by using a machine-learning-based approach, it has been shown that the discrimination of temperature, strain, and pressure could be possible (Lee et at., 2020). However, such approaches may require a considerable number of datasets for training to achieve high accuracy for identifying the mixed stimuli. In this aspect, when the multimodal sensors have inherent sensing capability of detecting various mixed stimuli independently, precise and accurate identification of each stimulus can be enabled.

Here, we report a textile-based multimodal sensor detecting strain and pressure simultaneously using silver nanowire (AgNW)/poly(3,4-ethylenedioxythiophene):poly(styrenesulfonate) (PEDOT:PSS)-coated conducting fibers and a high-k flexible ion-gel (IG) film. By utilizing the resistance variation of AgNW/PEDOT fiber depending on the applied strain, detection of strain up to 25% was possible. In addition, the capacitive structure of conducting fiber/IG film/conducting fiber enabled the detection of vertical pressure applied to the sensor. More importantly, it was observed that both the strain and pressure sensing can be performed simultaneously without being affected by other sensing stimuli. In this manner, separate detection and discrimination of strain and pressure was possible. Using the multimodal sensor integrated with one strain sensor and two pressure sensors, simultaneous detection of multiple weights was successfully carried out.
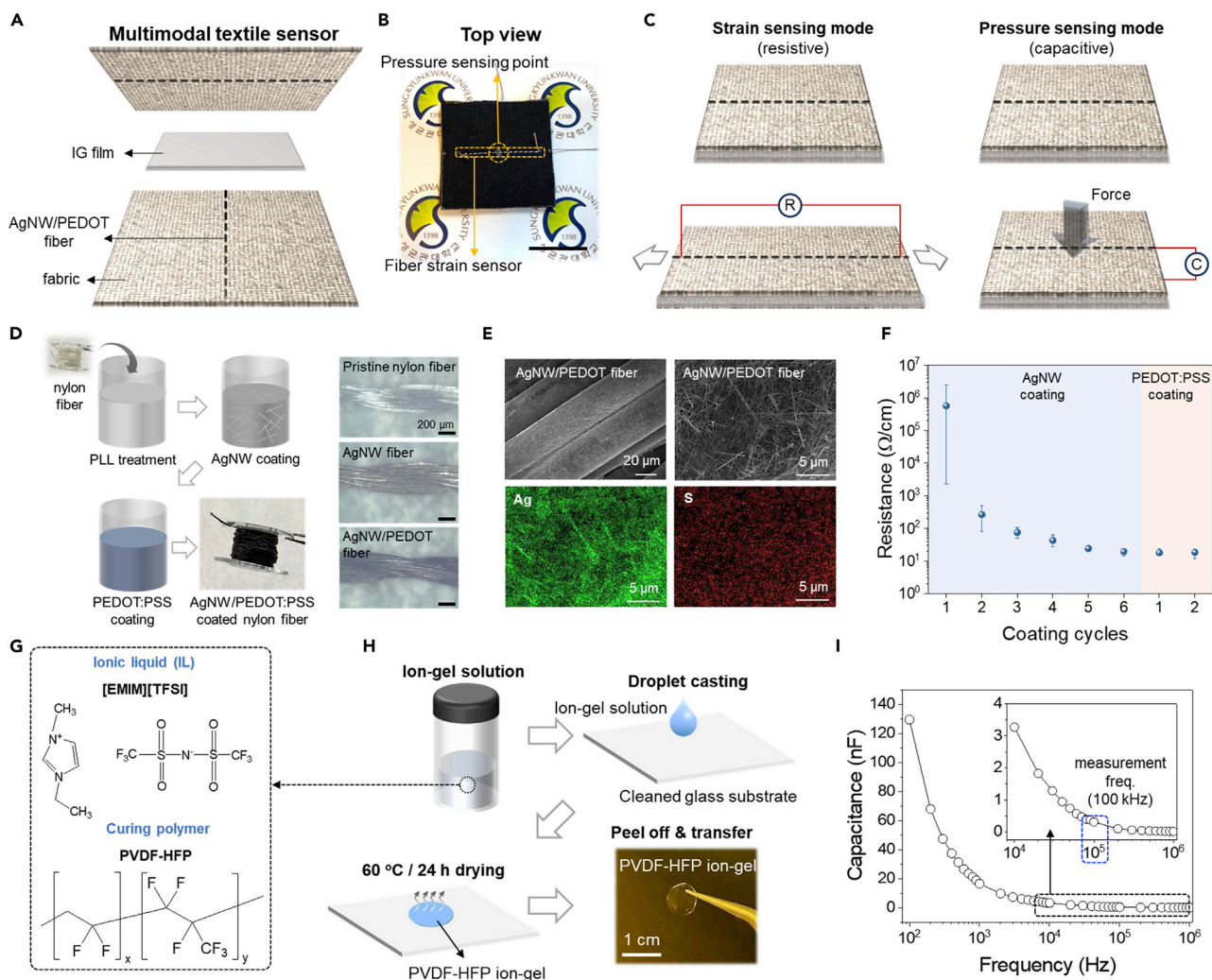
RESULTS

Device structure and fabrication of textile-based multimodal sensors

The structure and materials used for the fabrication of textile-based multimodal sensors are shown in Figure 1A. The multimodal sensor is composed of two fabric sheets with an IG film sandwiched between the fabrics. On each fabric, a AgNW/PEDOT conducting fiber is placed which is used as the strain-sensing element and an electrode. In addition, to form a capacitor structure for pressure detection, the AgNW/PEDOT fibers on top and bottom fabric sheets were orthogonally placed forming a cross-point. Figure 1B shows the fabricated textile-based multimodal sensor. For strain sensing, the resistance change of AgNW/PEDOT fiber upon stretching is utilized. In particular, because of the multifilament structure of AgNW/PEDOT fibers, the percolation between the monofilaments increases under a tensile strain, decreasing the resistance of AgNW/PEDOT fiber (Eom et at., 2017b). In addition, for pressure sensing, the capacitance variation of conducting fiber/IG film/conducting fiber capacitor is utilized. Here, when a pressure is applied to the sensor, the contact areas between the conducting fibers and the IG film are widened, increasing the capacitance value (Keum et al., 2021a). In this approach, the magnitude of applied pressure can be identified by monitoring the value of capacitance change. As described, the textile-based multimodal sensor can operate in strain-sensing mode and pressure-sensing mode as illustrated in Figure 1C.

Figure 1D shows the fabrication procedure of AgNW/PEDOT composite conducting fibers. Firstly, a pristine nylon fiber is immersed in a poly-L-lysine (PLL) solution to promote the adhesion of AgNWs on the nylon surface (Eom et at., 2017b). Next, the nylon fiber is dipped into a AgNW solution and thermally annealed. The dipping and annealing processes were repeated from one to six times. Afterward, the AgNW-coated nylon fiber (AgNW fiber) was dipped in a PEDOT:PSS solution and thermally annealed. The PEDOT:PSS coating was repeated from one to two times. The optical microscope images of nylon fibers after each coating process are shown in Figure 1D. The AgNW/PEDOT-coated nylon fiber (AgNW/PEDOT fiber) showed uniform dark blue color indicating that the AgNW and PEDOT:PSS are uniformly coated on the fiber. In addition, the multifilament structure of the fiber was maintained after the multiple coating processes. To further investigate the coating uniformity of AgNW and PEDOT:PSS on the fiber, the surface morphology and the distributions of silver (Ag) and sulfur (S) atoms were analyzed. Figure 1E shows the scanning electron microscopy (SEM) and corresponding energy dispersive X-ray spectroscopy (EDS) mapping images of AgNW/PEDOT fiber. As displayed in the SEM images, the AgNWs are uniformly coated on the fiber surface without noticeable aggregation. In addition, the EDS mapping images for Ag and S atoms support that the AgNWs and PEDOT:PSS are uniformly distributed on the fiber surface, respectively.

The electrical resistance and the uniformity largely varied with the number of AgNW and PEDOT:PSS coating processes. Figure 1F shows the variation of electrical resistance as functions of AgNW and PEDOT:PSS coating numbers. With a single AgNW coating, the resistance was relatively high and the

Figure 1. The structure of textile-based multimodal sensors and the fabrication processes of the AgNW/PEDOT fiber and the IG film

(A) The structure and materials used for the fabrication of textile-based multimodal sensors. The conducting AgNW/PEDOT fiber acts as the strain-sensing element and the conducting fiber/IG film/conducting fiber capacitor serves as the capacitive pressure-sensing element.

(B) Photographic image of the textile-based multimodal sensor. The scale bar indicates 2 cm.

(C) Strain-sensing (resistive) and pressure-sensing (capacitive) modes of the textile-based multimodal sensor.

(D) Fabrication procedure of the AgNW/PEDOT composite conducting fibers. The scale bars indicate 200 μm.

(E) SEM and corresponding EDS mapping images of AgNW/PEDOT composite fiber.

(F) The variation of electrical resistance as functions of AgNW and PEDOT:PSS coating numbers. The error bars indicate the distribution of resistance upon random ten points of AgNW/PEDOT composite fiber.

(G) The materials used to fabricate the flexible IG film. PVDF-HFP and [EMIM][TFSI] were used as curing polymers and ionic liquids, respectively.

(H) Fabrication procedure of the flexible IG film. The scale bar indicates 1 cm.

(I) The capacitance-frequency (C–F) characteristics of IG film in the range of 100 Hz ∼ 1 MHz. The inset shows the capacitance in the range of 10 kHz to 1 MHz.

uniformity was poor, showing resistance values in the range of 2.3×10^3–$2.5 \times 10^6 \, \Omega \, cm^{-1}$. As the number of AgNW coating processes increased, the average resistance and the uniformity were substantially improved. In particular, after six repeated coatings of AgNWs, the average resistance decreased down to $1.9 \times 10^1 \, \Omega \, cm^{-1}$ with a standard deviation of $2.35 \, \Omega \, cm^{-1}$. These improvements in the average resistance and the uniformity can be attributed to the increased numbers of AgNWs coated on the nylon fiber surface. Furthermore, additional coating of PEDOT:PSS decreased the resistance to $\sim 1.8 \times 10^1 \, \Omega \, cm^{-1}$. The coating of PEDOT:PSS had only a small influence on the resistance mainly because of relatively high resistivity of PEDOT:PSS compared to AgNWs (Fan et al., 2019). However, additional coating of
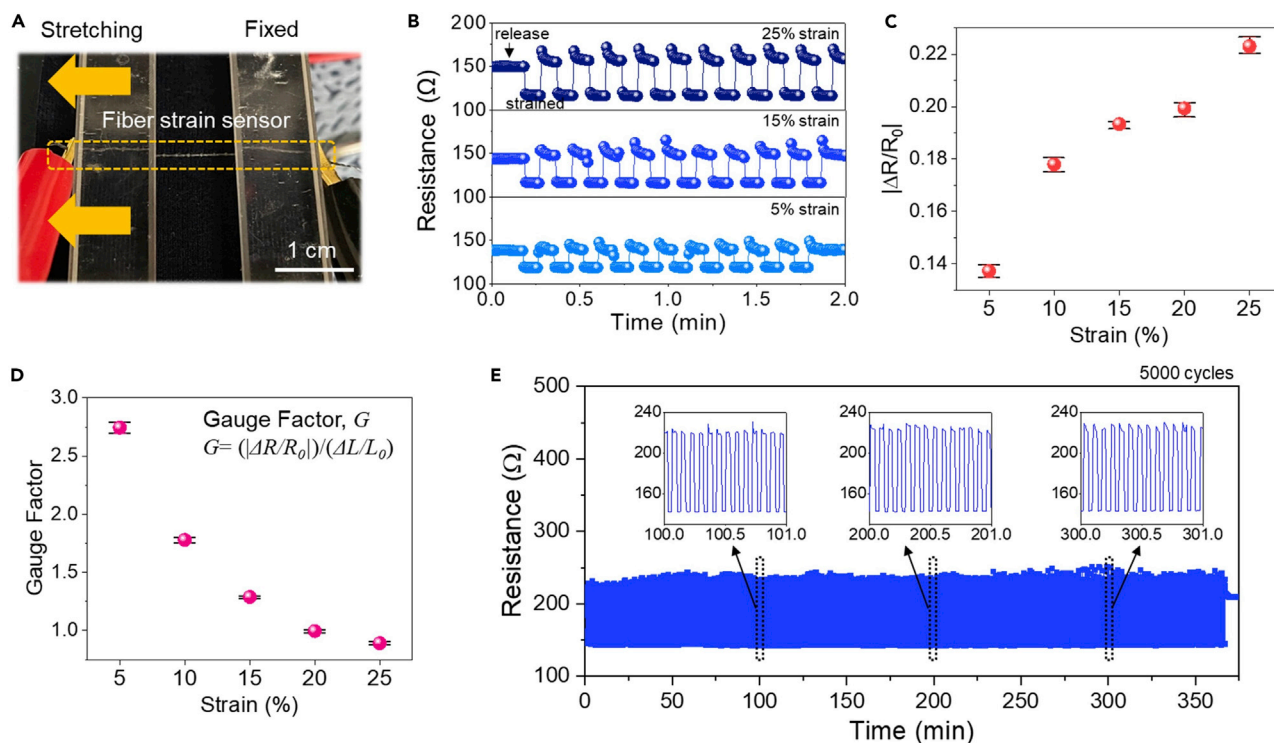
Figure 2. Strain-sensing characteristics and operational stability of textile-based multimodal sensor

(A) The measurement setup for strain-sensing characteristics.

(B) Resistance variation of AgNW/PEDOT fiber-based strain sensor upon ten stretch/release cycles. The applied strain levels were 5%, 15%, and 25%.

(C) Relative change of resistance ($|\Delta R/R_0|$) of the AgNW/PEDOT fiber-based strain sensor as a function of strain. The error bars indicate the distribution of $|\Delta R/R_0|$ upon ten cycles of stretching/releasing the test.

(D) The variation of gauge factor (G) as a function of strain. The error bars indicate the distribution of gauge factor upon ten cycles of stretching/releasing test.

(E) The variation of resistance during 5,000 stretch/release cyclic tests. Here, a strain of 20% was applied to the sensor.

PEDOT:PSS layer can induce enhanced adhesion of AgNWs on the nylon surface by conformally covering the AgNWs and prevent mechanical detachment during the subsequent fabrication processes.

To construct a capacitive pressure sensor, we used a flexible IG film as a dielectric, which was fabricated by using poly(vinylidene fluoride)-co-hexafluoropropylene (PVDF-HFP) and 1-ethyl-3-methylimidazolium bis(trifluoromethylsulfonyl)imide ([EMIM][TFSI]) as curing polymer and ionic liquid, respectively (Figure 1G). The IG solution was first dropped on a glass substrate and thermally cured. Afterward, the solid IG film was peeled off from the glass substrate and transferred onto the fabric sheet (Figure 1H). The capacitance-frequency (C-F) characteristics of IG film is shown in Figure 1I. Owing to the relatively slow migration of ionic liquid in the film, the capacitance value was decreased with the frequency. In the case of capacitive pressure sensor, to attain a high sensitivity, we selected an operating frequency of 100 kHz which exhibits a low initial capacitance value as shown in the inset of Figure 1I.

Strain-sensing characteristics and operational stability

At first, the strain-sensing characteristics of multimodal sensor were evaluated. As shown in Figure 2A, the textile sensor was mounted in a test fixture and the resistance was measured under different strain conditions. Here, the AgNW/PEDOT fiber sewn on the fabric had a linear pattern to obtain high strain sensitivity. In addition, to keep the pattern structure of AgNW/PEDOT fiber, an additional silver-plated fiber was used for the sewing process. The silver-plated fiber also forms a contact with the IG film for capacitive pressure sensing. Figure 2B shows the variation of resistance when 5, 15, and 25% of strain was applied to the sensor. In addition, Figure S1 shows the resistance variation under 10 and 20% of strain. Here, ten consecutive stretching and releasing were conducted to examine the repeatability of the sensor. Upon stretching, the resistance of the sensor decreased, whereas the magnitude of variation tended to increase with
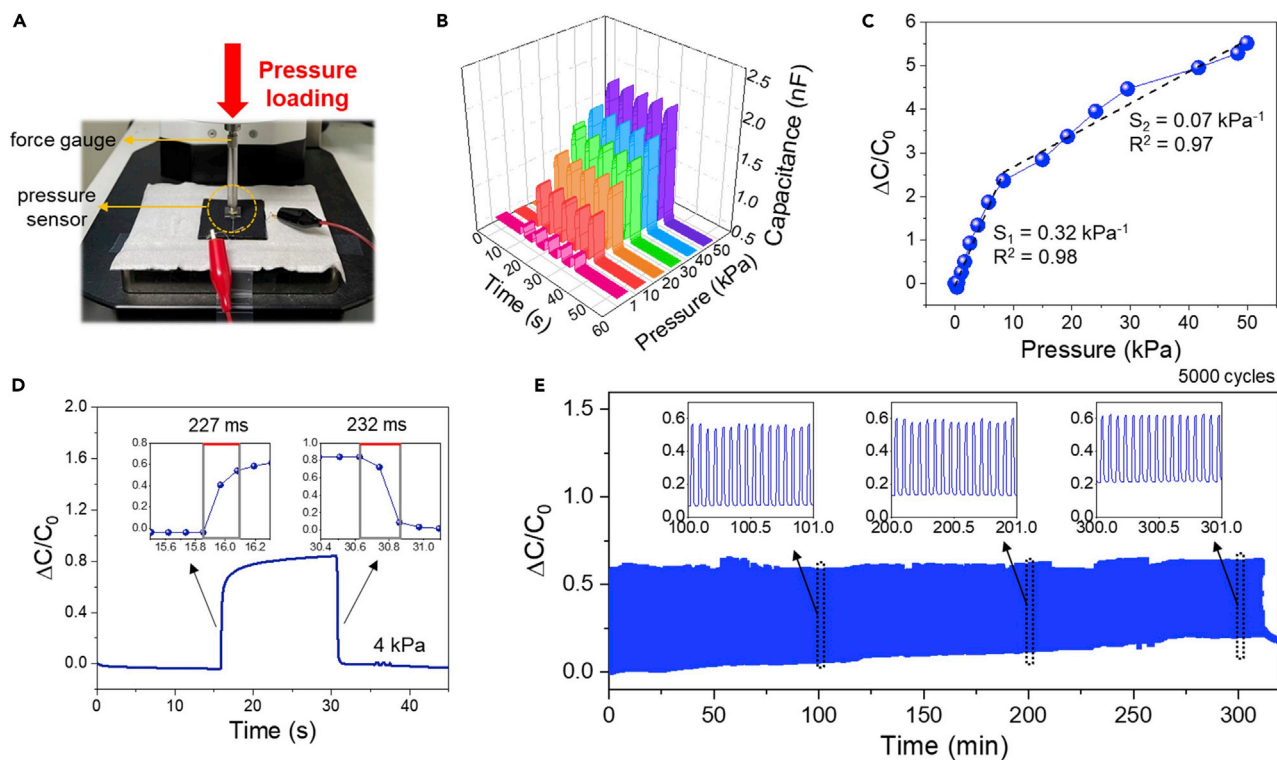
Figure 3. Pressure-sensing characteristics and operational stability of textile-based multimodal sensors

(A) The measurement setup for pressure-sensing characteristics using a force gauge.

(B) Capacitance variation of the IG-based pressure sensor upon five loading/unloading cycles with different levels of pressure.

(C) Pressure-sensing characteristics ($\Delta C/C_0$ vs. pressure) and sensitivity of the IG-based capacitive pressure sensor. Here, the applied pressure range was 1–50 kPa.

(D) Dynamic response characteristics of the IG-based pressure sensor and the response times for the loading and unloading.

(E) The variation of capacitance during 5,000 loading/unloading cyclic test. Here, a pressure of 1 kPa was applied to the sensor.

increasing strain. The decrease of resistance with the strain can be attributed to the multifilament structure of AgNW/PEDOT fibers. Specifically, when the fiber is stretched, the contact between the AgNW/PEDOT-coated nylon monofilaments is enhanced, generating more physical junctions between the monofilaments, decreasing the resistance of the fiber (Chawla et al., 2013; Zhang, 2015). Figure 2C shows the strain vs. resistance change ($|\Delta R/R_0|$) plot. In this strain range, the resistance tends to decrease with increasing strain. Particularly, when the strain was 5% and 25%, the $|\Delta R/R_0|$ values were 0.137 ± 0.002 and 0.223 ± 0.002, respectively. The results show that the amount of resistance change is almost linearly dependent on the applied strain and the variation of the change is small during repeated strain cycles, showing a high stability. Figure 2D shows the gauge factor (G) of the strain sensor as a function of applied strain. Here, the gauge factor was calculated by the following equation, $G = (|\Delta R|/R_0)/(\Delta L/L_0)$, where ΔL is the change in length and L_0 is the initial length. In the strain range of 5–25%, the gauge factor was 2.74–0.89, respectively. To further examine the reliability of AgNW/PEDOT fiber-based strain sensor, a stretch/release cyclic test was performed. Figure 2E shows the sensing performance for a total of 5,000 cycles at a strain level of 20%. It was observed that the sensing performance was stable without any significant changes in the resistance variation suggesting that the AgNWs and PEDOT:PSS are well adhered to the fiber during the mechanically stretched conditions.

Pressure-sensing characteristics and operational stability

Next, the performance of the capacitive pressure sensor was evaluated. In the IG-based capacitive pressure sensor, the capacitance value changes in accordance with the applied pressure. Figure 3A shows the pressure-sensing measurement system with the textile multimodal sensor placed under a force gauge. Programmed pressure is applied to the sensor and the capacitance variation was monitored using an LCR meter. Here, the conducting fibers on top and bottom fabrics were used as the counter electrodes

for the capacitor (Figure S2). Figures 3B and 3C and Figure S3 show the variation of capacitance as a function of pressure in a pressure range of 1–50 kPa. It is evident that the magnitude of capacitance change increased according to the pressure, which implies that the applied pressure can be identified. Particularly, in the pressure ranges of 1–10 kPa and 10–50 kPa, the sensor exhibited a sensitivity of 0.32 kPa^{-1} ($R^2 = 0.98$) and 0.07 kPa^{-1} ($R^2 = 0.97$), respectively. Here, the sensitivity was calculated using the equation, $S = (\Delta C/C_0)/\Delta P = ((C-C_0)/C_0)/(P-P_0)$. It should be noted that the fabricated textile pressure sensor can detect the pressure in a relatively wide range of pressures from 1 to 50 kPa with reasonably high sensitivity. This shows that diverse applications can be achieved using the IG-based pressure sensor which require different ranges of pressure detection. Also, the textile pressure sensor exhibited reasonably good repeatability (Figure 3B).

To determine the response time of the pressure sensor, an applied pressure of 4 kPa was loaded and the dynamic response characteristics were measured (Figure 3D). The response times extracted in the loading and unloading states were 227 ms and 232 ms, respectively, at a measurement frequency of 100 kHz (bias of 1 V). Considering the typical applications of textile pressure sensors for wearable electronics monitoring human body motion and various external stimuli, the response time can be sufficient for real-time detection. Furthermore, the operational stability of the pressure sensor was examined. The stability test was carried out by applying 1 kPa pressure to the sensor for 5,000 cycles. As shown in Figure 3E, the sensor was stably operated up to 5,000 cycles without significant failure, suggesting that the textile pressure sensor has good operational stability. To benchmark the performance of textile-based multimodal sensors with previously reported strain/pressure multimodal sensors, the strain gauge factor and the pressure sensitivity were compared as shown in Table S1. In the case of our textile-based multimodal sensor, the pressure sensitivity was relatively higher than those reported in the literature, with a moderate strain gauge factor. It is supposed that the low strain gauge factor can be attributed to the relatively high Young's modulus of nylon fiber which is used as the base material for the strain sensor. Furthermore, the multifilament structure of the fiber and the strain-dependent percolation conduction can also contribute to the relatively low gauge factor. In addition, it is to note that these previously reported sensors exhibited high strain gauge factors while having relatively low pressure sensitivity. To solve such issues, we implemented a high-κ ion-gel film as a pressure-sensing material. As a result, our textile-based multimodal sensor could simultaneously detect both the strain and pressure stimuli with reasonable sensing performances.

Strain/pressure multimodal sensing characteristics and mechanism

To investigate the multimodal sensing capability of the textile sensor, eight cycles of 5–25% of strain were applied to the sensor and the changes in the resistance and capacitance values were measured. Figure 4A shows the schematic illustration of the multimodal sensor operation. Figures 4B and 4D show the variations of both resistance and capacitance values during the strain cycles. In the measured strain range, it is apparent that the resistance of AgNW/PEDOT fiber varies according to the applied strain, whereas, the capacitance variation was negligible indicating that the influence of strain on the pressure-sensing characteristics is minimal. However, under 25% strain, a slight fluctuation of capacitance value was observed with maximum $\Delta C/C_0$ of ~0.01. It is expected that because of the longitudinally applied strain, a vertical force can be applied to the pressure sensor, resulting in a capacitance variation. However, the levels of $\Delta C/C_0$ caused by the strain is comparably smaller than those induced by typical pressures (Figure 1C), showing that the strain-sensing operation can be independently performed from the pressure sensing. Nevertheless, the strain sensor which is composed of AgNW/PEDOT fiber responds to the applied strain, whereas the IG-based pressure sensor is rather insensitive to the strain.

Furthermore, the influence of pressure on the resistive strain sensor was analyzed. As shown in Figure 4E, different levels of pressure were applied to the sensor and the variations of resistance and capacitance values were measured. As displayed in Figures 4F–4H, the resistance of the AgNW/PEDOT fiber-based strain sensor was not varied when low, medium, or high pressure was applied to the sensor. The variation of $\Delta C/C_0$ by different levels of pressure indicates that the pressure sensor is properly operated, capable of detecting the magnitude of applied pressure. This result states that the overall resistance of AgNW/PEDOT fiber is not severely affected by the vertical pressure. In addition, the AgNW/PEDOT fiber in the bottom fabric can also serve as a strain-sensing element (Figure 4I). Accordingly, the resistance variation of AgNW/PEDOT fiber in the bottom fabric was analyzed under identical pressure conditions. As shown in Figures 4J–4L, the bottom strain sensor was also unaffected by the pressure, showing that both strain
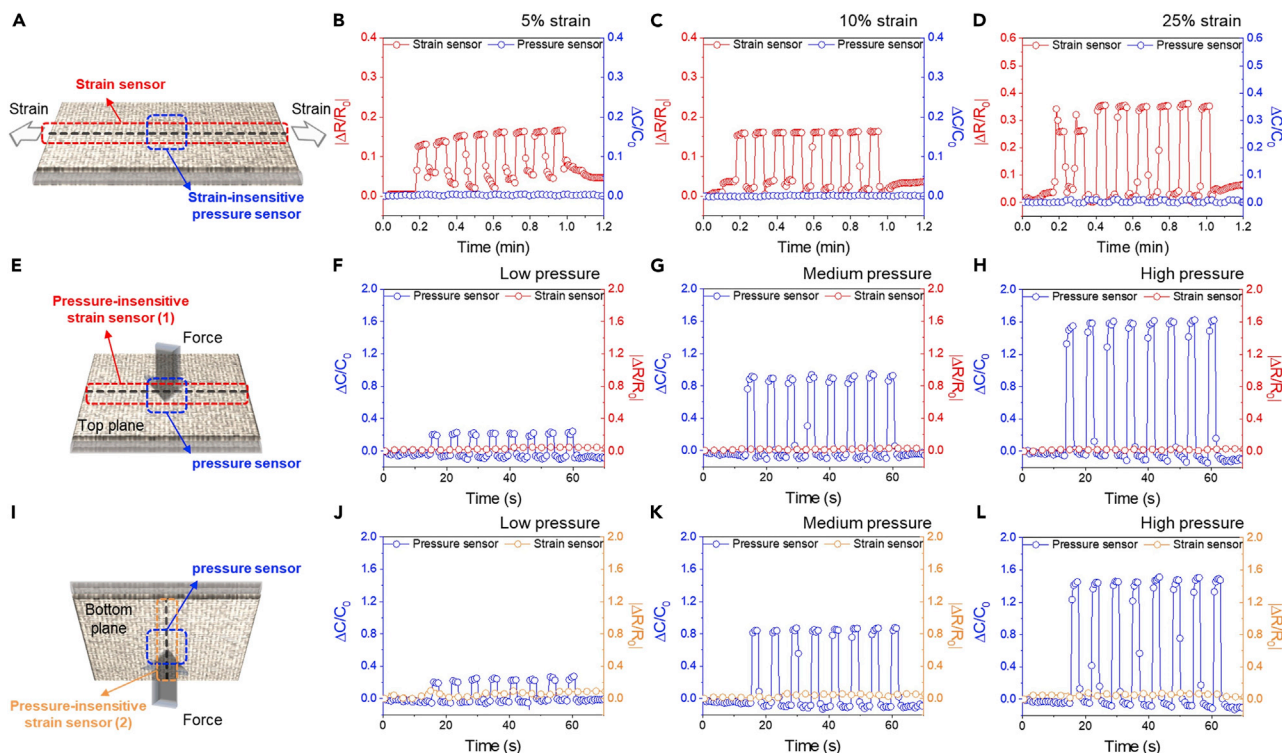
Figure 4. Strain/pressure multimodal sensing characteristics

(A) Schematic illustration of the multimodal sensing operation. The variation of resistance and capacitance values were monitored upon different levels of strain.

(B–D) The variations of resistance of strain sensor (red) and capacitance of pressure sensor (blue) during eight stretch/release cycles. Here, 5, 10, and 25% of strain were applied. During the strain cycle, the pressure sensor was insensitive to the applied strain.

(E) Schematic illustration of the multimodal sensing operation. The variation of resistance (top fabric) and capacitance values were monitored upon different levels of pressure.

(F–H) The variations of capacitance of pressure sensor (blue) and resistance of top strain sensor (red) during eight loading/unloading cycles. Here, low, medium, and high pressure was applied.

(I) Schematic illustration of the multimodal sensing operation. The variation of resistance (bottom fabric) and capacitance values were monitored upon different levels of pressure.

(J–L) The variations of capacitance of pressure sensor (blue) and resistance of bottom strain sensor (orange) during eight loading/unloading cycles. Here, low, medium, and high pressure was applied.

sensors can be independently operated from the capacitive pressure sensor. The details of strain/pressure multimodal sensing test setup are shown in Figures S4 and S5. Using this setup, the resistance and capacitance change through the two modes of operation of a textile-based multimodal sensor can be measured simultaneously.

The textile-based multimodal sensor detected strain through the resistance variation of AgNW/PEDOT fiber, and detected pressure through the capacitance variation of PVDF-HFP ion-gel capacitor. Through these two operation types, strain and pressure could be simultaneously detected with low signal interference independently. Figure 5 shows the strain and pressure-sensing mechanisms of the textile-based multimodal sensor. As shown in Figure 5A, the PVDF-HFP ion-gel film is located between two orthogonally crossed AgNW/PEDOT fiber strain sensors. First, as shown in Figure 5B, when a pressure is applied to the sensor, the contact area between PVDF-HFP ion-gel film and the fibers is enlarged. This caused an increase of surface electrical double layer (EDL) area, and consequently, the capacitance value. However, the resistance of AgNW/PEDOT strain sensors is not significantly affected by the pressure stimuli. In addition, when a tensile strain is applied to the sensor, the contacts between the AgNW/PEDOT monofilaments is enhanced as shown in Figure 5C. As a result, the overall resistance of the fiber is decreased. Then, when the strain is removed, the contact area between the monofilaments is recovered to the normal state; therefore, the resistance value is restored to its original value. In the case of
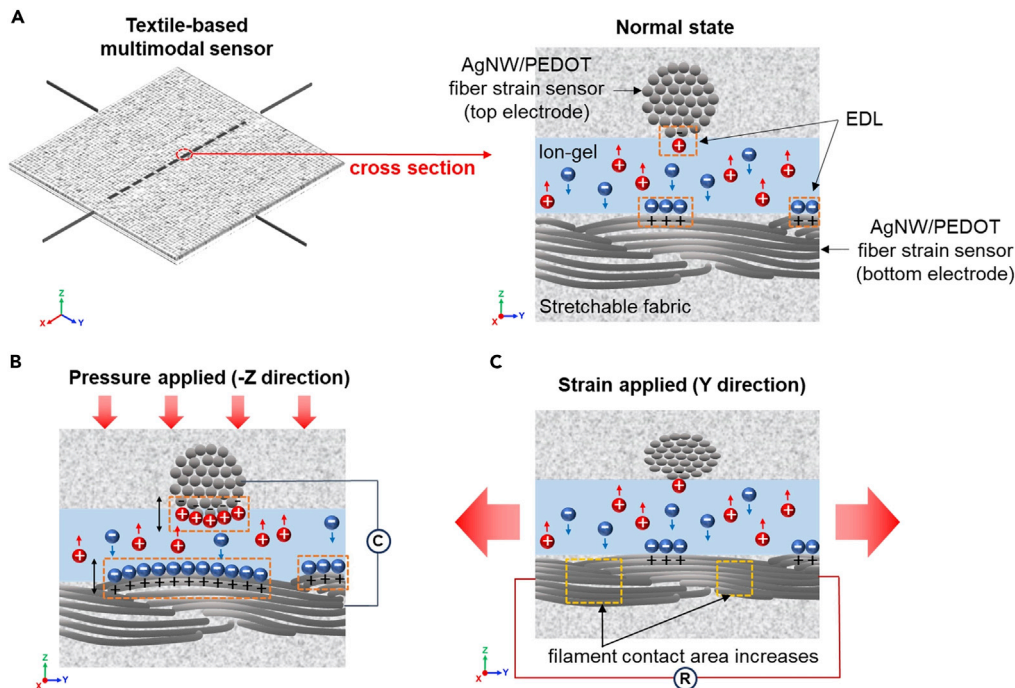
Figure 5. Strain and pressure-sensing mechanisms of a textile-based multimodal sensor
(A) Cross-section structure of the textile-based multimodal sensor.
(B) The pressure-sensing mechanism of the textile-based multimodal sensor. When a pressure is applied, the contact area of ion-gel film and AgNW/PEDOT fibers is enlarged, increasing the surface EDL area and the capacitance value.
(C) The strain-sensing mechanism of the textile-based multimodal sensor. When a strain is applied, the contact area between AgNW/PEDOT monofilaments is increased. As a result, the overall resistance of the fiber is decreased.

stretching and releasing, the area of EDL is not affected. As a result, the capacitance value is not changed by the strain. These two types of mechanism enable independent detection of pressure and strain stimuli.

To demonstrate the application of textile-based multimodal sensors, two IG-based capacitive pressure sensors were integrated in a single device. As shown in Figures 6A and 6B, the multimodal sensor was fabricated with one resistive strain sensor and two capacitive pressure sensors. Owing to the independent operation of each strain and pressure sensor, simultaneous monitoring of different pressures is possible using the sensor. Figure 6C shows the dynamic changes of capacitance and resistance variations for pressure sensor 1 and 2, and the strain sensor. On pressure sensor 1, a relatively heavy weight was loaded while a lighter weight was loaded on the pressure sensor 2. As displayed in Figure 6C, the determination of heavy and light weight pressure was possible by the different amounts of capacitance change. More importantly, the resistance response of the strain sensor was almost negligible by the loading of the weights. From these observations, it is apparent that the strain and pressure sensors can be independently operated in a single device, which can be utilized as a multimodal sensor detecting strain and pressure for wearable electronics.

DISCUSSION

Here, we demonstrated a textile-based multimodal sensor capable of simultaneously and independently strain and pressure in a single device. The textile-based multimodal sensor consists of AgNW/PEDOT fiber strain sensor operated with resistance change, and IG-based pressure sensor operated with capacitance change. The AgNW/PEDOT fiber strain sensor showed a gauge factor up to 2.74, and the IG-based pressure sensor showed a sensitivity up to 0.32 kPa^{-1}. Also, both sensors were mechanically robust without significant deterioration or fracture during cyclic tests. In addition, the textile-based multimodal sensor exhibited individual operation of strain and pressure sensing without signal interference between the stimuli.
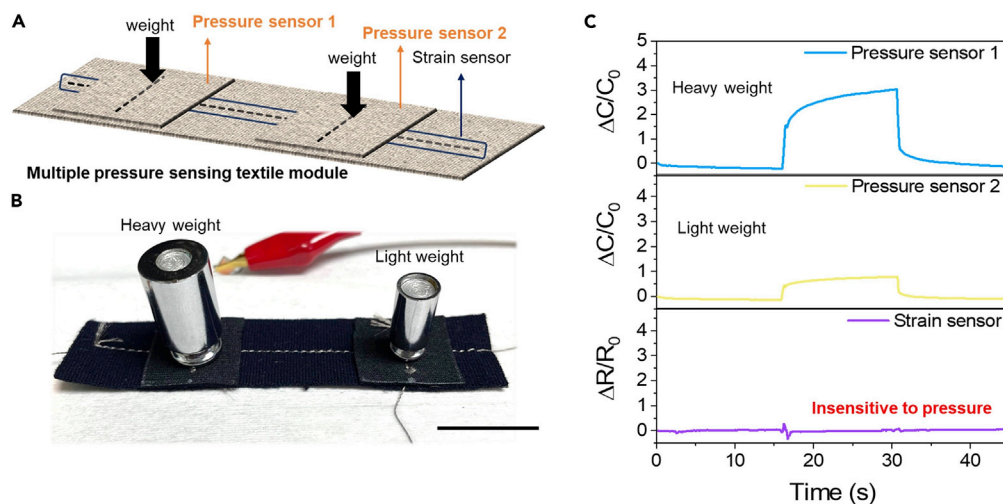
Figure 6. Simultaneous detection of multiple weights using the textile-based multimodal sensor

(A) The schematic illustration of the textile-based multimodal sensor having two capacitive pressure sensors and one resistive strain sensor.

(B) The photograph of textile-based multimodal sensor loaded with heavy and light weights on pressure sensor 1 and 2, respectively. The scale bar indicates 2 cm.

(C) Dynamic changes of capacitance and resistance values for pressure sensors 1 and 2, and the strain sensor. The pressure sensor 1 was loaded with a heavy weight and showed a larger capacitance change. On the pressure sensor 2, a light weight was loaded and showed a smaller capacitance change.

Finally, we successfully demonstrated multiple weight sensing using the textile-based multimodal sensor. Here, simultaneous detection of different weights was enabled by the integrated pressure sensors in a single unit module. From these results, we envision that the textile-based multimodal sensor can be promising in realizing various potential applications in wearable smart clothing and smart textiles where simultaneous multi-signal detection is required.

Limitations of the study

In addition to strain and pressure, other external stimuli such as bending, temperature, and chemical species could also affect the sensing characteristics. In particular, the bending of the fabric can also cause localized strain and pressure to the sensor devices and change the resistance and capacitance values. Also, the temperature change may induce a change in the resistivity of the AgNW/PEDOT conducting fibers. As a result, the main limitation of this study is that the correlations between various external stimuli such as bending, temperature, and chemical species needed to be identified further to fully identify and discriminate each incoming stimulus. In future research, we aim to investigate the correlations and interference between external stimuli for textile-based wearable electronics.

STAR★METHODS

Detailed methods are provided in the online version of this paper and include the following:

- KEY RESOURCES TABLE
- RESOURCE AVAILABILITY
  - Lead contact
  - Materials availability
  - Data and code availability
- METHOD DETAILS
  - Fabrication of AgNW/PEDOT conducting fibers and textile-based strain sensors
  - Fabrication of PVDF-HFP IG film and textile-based multimodal sensors
  - Characterization of materials and multimodal sensors
- QUANTIFICATION AND STATISTICAL ANALYSIS

AUTHOR CONTRIBUTIONS

K.K., S.K.P. and Y.H.K. conceptualized and designed the project. K.K. and Y.H.K. designed and performed most of the experiments and analysis. S.S.C. and J.-W.J. performed the analysis of the data. K.K., S.K.P. and Y.H.K. prepared the original draft, and reviewed and edited the final draft.

DECLARATION OF INTERESTS

The authors declare no competing interests.

SUPPORTING CITATIONS

Cheng et al., 2017; He et al., 2020; Huang et al., 2020; Kim et al., 2018a; Kim et al., 2018b; Ma et al., 2021; Qin et al., 2020; Shin et al., 2019; Wang et al., 2020.

REFERENCES

Agcayazi, T., Tabor, J., McKnight, M., Martin, I., Ghosh, T.K., and Bozkurt, A. (2020). Fully-textile seam-line sensors for facile textile integration and tunable multi-modal sensing of pressure, humidity, and wetness. Adv. Mater. Technol. 5, 2000155.

Chawla, S., Naraghi, M., and Davoudi, A. (2013). Effect of twist and porosity on the electrical conductivity of carbon nanofiber yarns. Nanotechnology 24, 255708.

Chen, Q., Tang, H., Liu, J., Wang, R., Sun, J., Yao, J., Shao, Z., and Chen, X. (2021). Silk-based pressure/temperature sensing bimodal ionotronic skin with stimulus discriminability and low temperature workability. Chem. Eng. J. 422, 130091.

Chen, S., Peng, S., Sun, W., Gu, G., Zhang, Q., and Guo, X. (2019). Scalable processing ultrathin polymer dielectric films with a generic solution based approach for wearable soft electronics. Adv. Mater. Technol. 4, 1800681.

Cheng, Y., Wang, R., Zhai, H., and Sun, J. (2017). Stretchable electronic skin based on silver nanowire composite fiber electrodes for sensing pressure, proximity, and multidirectional strain. Nanoscale 9, 3834.

Eom, J., Heo, J.-S., Kim, M., Lee, J.H., Park, S.K., and Kim, Y.-H. (2017b). Highly sensitive textile-based strain sensors using poly(3,4-ethylenedioxythiophene):polystyrene sulfonate/silver nanowire-coated nylon threads with poly-L-lysine surface modification. RSC Adv. 7, 53373–53378.

Eom, J., Jaisutti, R., Lee, H., Lee, W., Heo, J.-S., Lee, J.-Y., Park, S.K., and Kim, Y.-H. (2017a). Highly sensitive textile strain sensors and wireless user-interface devices using all-polymeric conducting fibers. ACS Appl. Mater. Inter. 9, 10190–10197.

Fan, X., Nie, W., Tsai, H., Wang, N., Huang, H., Cheng, Y., Wen, R., Ma, L., Yan, F., and Xia, Y. (2019). PEDOT:PSS for flexible and stretchable electronics: modifications, strategies, and applications. Adv. Sci. 6, 1900813.

He, F., You, X., Gong, H., Yang, Y., Bai, T., Wang, W., Guo, W., Liu, X., and Ye, M. (2020). Stretchable, biocompatible, and multifunctional silk fibroin-based hydrogels toward wearable strain/pressure sensors and triboelectric nanogenerators. ACS Appl. Mater. Inter. 12, 6442–6450.

Ho, D.H., Cheon, S., Hong, P., Park, J.H., Suk, J.W., Kim, D.H., Han, J.T., and Cho, J.H. (2019). Multifunctional smart textronics with blow-spun nonwoven fabrics. Adv. Funct. Mater. 29, 1900025.

Huang, J., Zhao, M., Cai, Y., Zimniewska, M., Li, D., and Wei, Q. (2020). Dual-mode wearable sensor based on bacterial cellulose reinforced hydrogels for highly sensitive strain/pressure sensing. Adv. Electron. Mater. 6, 1900934.

Kang, S.-K., Murphy, R.K.J., Hwang, S.-W., Lee, S.M., Harburg, D.V., Krueger, N.A., Shin, J., Gamble, P., Cheng, H., Yu, S., et al. (2016). Bioresorbable silicon electronic sensors for the brain. Nature 530, 71–76.

Keum, K., Eom, J., Lee, J.H., Heo, J.S., Park, S.K., and Kim, Y.-H. (2021a). Fully-integrated wearable pressure sensor array enabled by highly sensitive textile-based capacitive ionotronic devices. Nano Energy 79, 105479.

Keum, K., Heo, J.S., Eom, J., Lee, K.W., Park, S.K., and Kim, Y.-H. (2021b). Highly sensitive textile-based capacitive pressure sensors using PVDF-HFP/ionic liquid composite films. Sensors 21, 442.

Kim, H., Shaqeel, A., Han, S., Kang, J., Yun, J., Lee, M., Lee, S., Kim, J., Noh, S., Choi, M., et al. (2021). In situ formation of Ag nanoparticles for fiber strain sensors:toward textile-based wearable applications. ACS Appl. Mater. Inter. 13, 39868–39879.

Kim, S.J., Song, W., Yi, Y., Min, B.K., Mondal, S., An, K.-S., and Choi, C.-G. (2018a). High durability and waterproofing rGO/SWCNT-fabric-based multifunctional sensors for human-motion detection. ACS Appl. Mater. Inter. 10, 3921–3928.

Kim, M.-G., Alrowais, H., and Brand, O. (2018b). 3D-Integrated and multifunctional all-soft physical microsystems based on liquid metal for electronic skin applications. Adv. Electron. Mater. 4, 1700434.

Lee, J.H., Heo, J.S., Kim, Y.-J., Eom, J., Jung, H.J., Kim, J.-W., Kim, I., Park, H.-H., Mo, H.S., Kim, Y.-H., et al. (2020). A behavior-learned cross-reactive sensor matrix for intelligent skin perception. Adv. Mater. 32, 2000969.

Lee, J., Kwon, H., Seo, J., Shin, S., Koo, J.H., Pang, C., Son, S., Kim, J.H., Jang, Y.H., Kim, D.E., et al. (2015). Conductive fiber-based ultrasensitive

textile pressure sensor for wearable electronics. Adv. Mater. 27, 2433–2439.

Luo, S., Zhou, X., Tang, X., Li, J., Wei, D., Tai, G., Chen, Z., Liao, T., Fu, J., Wei, D., et al. (2021). Microconformal electrode-dielectric integration for flexible ultrasensitive robotic tactile sensing. Nano Energy 80, 105580.

Ma, L., Wu, R., Patil, A., Zhu, S., Meng, Z., Meng, H., Hou, C., Zhang, Y., Liu, Q., Yu, R., et al. (2019). Full-textile wireless flexible humidity sensor for human physiological monitoring. Adv. Funct. Mater. 29, 1904549.

Ma, Y., Ouyang, J., Raza, T., Li, P., Jian, A., Li, Z., Liu, H., Chen, M., Zhang, X., Qu, L., et al. (2021). Flexible all-textile dual tactile-tension sensors for monitoring athletic motion during taekwondo. Nano Energy 85, 105941.

Pyo, S., Lee, J., Kim, W., Jo, E., and Kim, J. (2019). Multi-layered, hierarchical fabric-based tactile sensors with high sensitivity and linearity in ultrawide pressure range. Adv. Funct. Mater. 29, 1902484.

Qi, K., Zhou, Y., Ou, K., Dai, Y., You, X., Wang, H., He, J., Qin, X., and Wang, R. (2020). Weavable and stretchable piezoresistive carbon nanotubes-embedded nanofiber sensing yarns for highly

sensitive and multimodal wearable textile sensor. Carbon 170, 464–476.

Qin, Z., Sun, X., Yu, Q., Zhang, H., Wu, X., Yao, M., Liu, W., Yao, F., and Li, J. (2020). Carbon nanotubes/hydrophobically associated hydrogels as ultrastretchable, highly sensitive, stable strain, and pressure sensors. ACS Appl. Mater. Inter. 12, 4944–4953.

Shin, S.-H., Lee, W., Kim, S.-M., Lee, M., Koo, J.M., Hwang, S.Y., Oh, D.X., and Park, J. (2019). Ion-conductive self-healing hydrogels based on an interpenetrating polymer network for a multimodal sensor. Chem. Eng. J. 371, 452–460.

Trung, T.Q., Ramasundaram, S., Hwang, B.-U., and Lee, N.-E. (2016). An all-elastomeric transparent and stretchable temperature sensor for body-attachable wearable electronics. Adv. Mater. 20, 502–509.

Wang, L., Wang, D., Wu, Z., Luo, J., Huang, X., Gao, Q., Lai, X., Tang, L.-C., Xue, H., and Gao, J. (2020). Self-derived superhydrophobic and multifunctional polymer sponge composite with excellent joule heating and photothermal performance for strain/pressure sensors. ACS Appl. Mater. Interf. 12, 13316–13326.

Wu, R., Ma, L., Hou, C., Meng, Z., Guo, W., Yu, W., Yu, R., Hu, F., and Liu, X.Y. (2019). Silk composite

electronic textile sensor for high space precision 2D combo temperature–pressure sensing. Small 15, 1901558.

Yang, S., Li, C., Wen, N., Xu, S., Huang, H., Cong, T., Zhao, Y., Fan, Z., Liu, K., and Pan, L. (2021). All-fabric-based multifunctional textile sensor for detection and discrimination of humidity, temperature, and strain stimuli. J. Mater. Chem. C 9, 13789–13798.

You, I., Mackanic, D.G., Matsuhisa, N., Kang, J., Kwon, J., Beker, L., Mun, J., Suh, W., Kim, T.Y., Tok, J.B.-H., et al. (2021). Artificial multimodal receptors based on ion relaxation dynamics. Science 370, 961–965.

Zhang, H. (2015). Flexible textile-based strain sensor induced by contacts. Meas. Sci. Technol. 26, 105102.

Zhou, G., Byun, J.-H., Oh, Y., Jung, B.-M., Cha, H.-J., Seong, D.-G., Um, M.-K., Hyun, S., and Chou, T.-W. (2017). Highly sensitive wearable textile-based humidity sensor made of high-strength, single-walled carbon nanotube/poly(vinyl alcohol) filaments. ACS Appl. Mater. Inter. 9, 4788–4797.

Zhu, Z., Li, R., and Pan, T. (2017). Imperceptible epidermal–iontronic interface for wearable sensing. Adv. Mater. 30, 1705122.

STAR★METHODS

KEY RESOURCES TABLE

REAGENT or RESOURCE	SOURCE	IDENTIFIER
Chemicals, peptides, and recombinant proteins		
Poly(vinylidene fluoride)-co-hexafluoropropylene	Sigma-Aldrich	CAS Number: 9011-17-0
1-ethyl-3-methylimidazolium bis(trifluoromethylsulfonyl)imide	Sigma-Aldrich	CAS Number: 174899-82-2
Silver nanowire ink	Ditto Technol.	CAS Number: 7440-22-4
Poly(3,4-ethylenedioxythiophene):polystyrene sulfonate	Sigma-Aldrich	CAS Number: 155090-83-8
Poly-L-lysine	Sigma-Aldrich	CAS Number: 25988-63-0
Software and algorithms		
Origin 2017	OriginLab	www.originlab.com
Clarius+	Tektronix	www.tek.com/en
MESUR Lite	Mark-10	mark-10.com
Other		
Optical microscopy	Leica	DM LM
Field-emission scanning electron microscope	JEOL	JSM-7600F
Source measure unit	Tektronix	Keithley 2400
Strain/bending stage	JAEIL optical system	J9141
LCR meter	Agilent	4284A
Semiconductor parameter analyzer	Tektronix	Keithley 4200A-SCS
Digital force gauge	Mark-10	M5-5
Tensile compression stand	Mark-10	ESM-303

RESOURCE AVAILABILITY

Lead contact

Further information and requests for resources and reagents should be directed to and will be fulfilled by the lead contact, Prof. Yong-Hoon Kim (yhkim76@skku.edu.)

Materials availability

This study did not generate new unique reagents.

Data and code availability

Data reported in this paper will be shared by the lead contact upon request. This paper does not report original code. Any additional information required to reanalyze the data reported in this paper is available from the lead contact upon request.

METHOD DETAILS

Fabrication of AgNW/PEDOT conducting fibers and textile-based strain sensors

The AgNW/PEDOT fiber was fabricated by the dip-coating method (Eom et al., 2017b). First, a commercial multifilament nylon fiber was prepared and sonicated with ethanol, methanol and de-ionized water for 10 min each and completely dry in a convection oven at 80°C for 3 h. Next, a poly-L-lysine (PLL) surface treatment was performed by immersing the nylon fiber in an aqueous PLL solution (0.1 w/vol% in H_2O, purchased from Sigma Aldrich and used without any purification) for 1 h. Afterward, the PLL-treated nylon fiber was blown with a nitrogen gun and dipped in an AgNW ink (1% ethanol dispersion, purchased from Ditto. Technol.) for 10 min and dried at 80°C for 20 min in a vacuum oven. To obtain high electrical conductivity,

AgNW coating and drying processes were repeated up to six times. Next, for the PEDOT:PSS coating, the AgNW-coated nylon fiber was dipped in a PEDOT:PSS solution (1.1% in H_2O, neutral pH, purchased form Sigma Aldrich and used without any purification) for 20 min and dried at 100°C for 20 min in a vacuum oven. The coating of PEDOT:PSS was repeated up to two times. The textile-based strain sensor was fabricated using the AgNW/PEDOT conducting fiber. The AgNW/PEDOT fiber was mechanically sewn onto a stretchable polyester fabric using a digital automatic embroidery sewing machine (Brother, Innovis 55p) with a linear pattern.

Fabrication of PVDF-HFP IG film and textile-based multimodal sensors

A freestanding PVDF-HFP IG film was fabricated by a droplet drop-casting method (Keum et al., 2021b). At first, PVDF-HFP pellets (average M_w ∼455,000, purchased from Sigma Aldrich) were dissolved in acetone (12 wt % of PVDF-HFP) and stirred for 4 h to prepare the PVDF-HFP solution. Then, the PVDF-HFP solution and 1-ethyl-3-methylimidazolium bis(trifluoromethylsulfonyl)imide ([EMIM][TFSI]) ionic liquid (≥98%, M_w = 391.31, purchased from Sigma Aldrich) were mixed at a weight ratio of 6.5:3.5 and stirred for 1 h. Next, the IG solution was dropped on a glass substrate with a volume of 10 µL. For the curing of IG film, thermal drying was carried out at 70°C for 24 h in a vacuum oven. After drying, the IG film was peeled off from the glass substrate. For the fabrication of textile-based multimodal sensor, two fabric sheets having AgNW/PEDOT fibers were prepared and the PVDF-HFP IG film was placed on the center region where two AgNW/PEDOT conducting fibers are present (top and bottom of the IG film). Here, an adhesive film (3M, 9472, 0.13 mm-thick) was used to attach the fabric sheets.

Characterization of materials and multimodal sensors

The surface morphology of multifilament AgNW/PEDOT conducting fibers and energy dispersive X-ray spectroscopy (EDS) spectra were analyzed using a field-emission scanning electron microscope (JEOL, JSM-7600F). The electrical resistance of AgNW/PEDOT fiber-based strain sensor was measured using a source measure unit (Keithley, model 2400). The capacitance properties of textile-based multimodal sensor were analyzed using an LCR meter (Agilent Technologies, Inc., 4284A) and a semiconductor parameter analyzer (Keithley, 4200A-SCS). To apply strain to the textile-based multimodal sensor, we utilized a homemade strain testing equipment. Also, to apply pressure to the multimodal sensor, a digital force gauge (M5-5, MARK-10) was used. The capacitance value of the textile-based multimodal sensor was measured at a frequency of 100 kHz with an applied voltage of 1 V AC.

QUANTIFICATION AND STATISTICAL ANALYSIS

Figure 1F indicated the average value of the resistance of ten random points of the AgNW/PEDOT fiber and the error bars correspond to the maximum and minimum values of the measured resistance respectively. This statistical process was done to confirm the uniformity over the number of coatings. In addition, Figures 2C and 2D indicated the average values of $|\Delta R/R_0|$ and the gauge factor obtained from the resistance change in ten cycles of stretching/releasing in Figure 2B, respectively. The error bars in Figures 2C and 2D show the standard deviation. All the statistical data were processed through the Origin software.